THE ASTROPHYSICAL JOURNAL, 507:L109–L112, 1998 November 10


# FILAMENTS AND PANCAKES IN THE *IRAS* 1.2 Jy REDSHIFT CATALOG

B. S. SATHYAPRAKASH,[1] VARUN SAHNI,[2] SERGEI SHANDARIN,[3] AND KARL B. FISHER[4]

*Received 1998 May 19; accepted 1998 September 8; published 1998 September 30*

## ABSTRACT

We explore the shapes of clusters and superclusters in the *IRAS* 1.2 Jy redshift survey with three reconstructions spanning the range $\beta = 0.1$, 0.5, and 1.0, where $\beta = \Omega^{0.6}/b$; $b$ is the bias factor, and $\Omega$ is the present value of the dimensionless matter density. Comparing our results with Gaussian randomized reconstructions of the *IRAS* catalog, we find structures having both planar and filamentary properties. For $\beta = 0.5$ and 1.0, the *largest structures in the survey have a distinct tendency to be filament-like*, in general agreement with the results of *N*-body simulations.

*Subject headings:* cosmology: theory — galaxies: clusters: general — infrared: galaxies — large-scale structure of universe — methods: analytical — methods: numerical

Redshift surveys of galaxies show that the large-scale structure of the Universe has a nonrandom pattern that, on different occasions, has been described as being cellular, network-like, filamentary, a cosmic web, etc. (Zeldovich, Einasto, & Shandarin 1982; de Lapparent, Geller, & Huchra 1991; Bond, Kofman, & Pogosyan 1996). It is also well known that individual structures forming through gravitational instability are likely to be anisotropic since gravitational instability leads generically to a collapse along one dimension, resulting in the formation of pancakes (Shandarin & Zeldovich 1989; Shandarin et al. 1995); moreover, with the passage of time, filamentary features acquire greater prominence, and the large-scale distribution develops a network-like structure (Yess & Shandarin 1996; Sathyaprakash, Sahni, & Shandarin 1996).

The geometrical properties of large-scale structure have evoked great interest in recent years, and mathematical tools as diverse as minimal spanning trees, genus curves, percolation theory, Minkowski functionals, and shape statistics have all been employed in their study. The necessity of using different statistical measures to study large-scale structure arises because traditional indicators of clustering, such as the two-point correlation function, though robust, do not address the issue of "connectedness" or shape, issues that are central to an integral understanding of the morphology of large-scale structure and of the physics of gravitational clustering (Sahni & Coles 1995).

Some key issues of the large-scale clustering of matter, such as whether the Great Wall in the north and the Sculptor Wall in the south are truly one-dimensional "filaments" or whether they are part of a more complex cellular structure consisting of sheets and bubbles of which they represent a limited slice, will be addressed by forthcoming large-redshift surveys, such as the Sloan Digital Sky Survey (SDSS) and the Two-Degree Field (2dF). In the present Letter, we report some progress toward this goal by analyzing the shapes of clusters and superclusters in the *IRAS* 1.2 Jy redshift survey.

Percolation theory, when applied to gravitationally clustered systems, suggests that most of the matter is likely to be concentrated in pancakes, filaments, and ribbons since such an arrangement percolates easily (i.e., at small values of the filling factor), as borne out by *N*-body simulations showing that the filling factor at percolation for cold dark matter–type models can be as low as 3%–5%, down from 16% for a Gaussian random field (Klypin & Shandarin 1993). Percolation analysis has also shown that the number of distinct clusters in a continuous density distribution peaks just before the onset of percolation. Thus, the percolation transition presents a natural threshold at which to study the shapes of individual clusters (Sathyaprakash et al. 1996, 1998), and in our study we shall employ this threshold to study clusters in the *IRAS* survey. In a companion paper (Sathyaprakash et al. 1998), we have made an exhaustive analysis of the robustness of the shape statistic to the threshold by studying the shapes of clusters defined at different density thresholds. The results of that analysis indicated that the modified shape statistic of Babul & Starkman (1992) gives qualitatively similar results for clusters defined according to different criteria. In the present Letter, we shall quote results for clusters defined at the percolation threshold since the results of Yess & Shandarin (1996) and Sathyaprakash et al. (1996, 1998) lead us to believe that the latter provides a robust and practically useful threshold at which to study shapes. (A comprehensive analysis of the *IRAS* 1.2 Jy redshift survey using percolation theory was carried out by Yess, Shandarin, & Fisher 1997.)

We shall analyze clusters in the *IRAS* 1.2 Jy redshift survey using a moment-based shape statistic that was originally suggested for a distribution of points by Babul & Starkman (1992, hereafter BS) and modified for use on continuous density distributions by Sathyaprakash et al. (1996). We briefly describe the modified version of the BS statistic before applying it to clusters obtained at the percolation threshold using a nearest-neighbors algorithm. In order to minimize fluctuations, our cluster-finding algorithm uses six nearest neighbors. However, detailed properties of a cluster could depend, in general, on the method used to identify clusters. This is an issue that requires further scrutiny, and a comprehensive analysis of the sensitivity of genus, percolation, and shape statistics to the nearest-neighbor algorithm (used to define clusters) will be discussed in a future work. Since the *IRAS* catalog does not cover the full sky, it is relevant to ask whether edge and boundary effects could have crept into the present analysis. Although a quantitative assessment of these effects lies outside the scope of this

[1] Department of Physics and Astronomy, Cardiff University, Cardiff, CF2 3YB, Wales, UK.
[2] Inter-University Centre for Astronomy and Astrophysics, Post Bag 4, Ganeshkhind, Pune-411007, India.
[3] Department of Physics and Astronomy, University of Kansas, Lawrence, KS 66045.
[4] Institute for Advanced Studies, Olden Lane, Natural Sciences, Building E, Princeton, NJ 08540.

Letter, a visual inspection of clusters and superclusters shows that the effect of boundaries in distorting shape is rather small.

Let $\rho(\boldsymbol{x})$ be the density field of matter distribution defined on a grid with coordinates $\boldsymbol{x}^p = (x_1^p, x_2^p, x_3^p)$, $p = 1, \ldots, N$. The first and second moments of the density distribution around a fiducial point $\boldsymbol{x}^0$ are given by

$$M_i(\boldsymbol{x}^0;\ R) = \frac{1}{\mathcal{M}} \sum_{p=1}^{N} y_i^p \rho(\boldsymbol{x}^p) W(|\boldsymbol{y}^p|), \tag{1}$$

$$M_{ij}(\boldsymbol{x}^0;\ R) = \frac{1}{\mathcal{M}} \sum_{p=1}^{N} y_i^p y_j^p \rho(\boldsymbol{x}^p) W(|\boldsymbol{y}^p|), \tag{2}$$

where $i, j = 1, 2, 3$, $R$ is the radius of a window $W$ centered on the point $\boldsymbol{x}^0$, $\boldsymbol{y}^p \equiv \boldsymbol{x}^p - \boldsymbol{x}^0$ is the coordinate of the $p$th grid point relative to the fiducial point $\boldsymbol{x}^0$, and $\mathcal{M}$ is the total mass in a given region:

$$\mathcal{M} = \sum_{p=1}^{N} \rho(\boldsymbol{x}^p) W(|\boldsymbol{x}^p - \boldsymbol{x}^0|). \tag{3}$$

In this study, we use a spherical top-hat window function that is large enough to cover the entire cluster under study. Also, the fiducial point is chosen to be the center of mass of the cluster in question. The moment-of-inertia tensor $I_{ij}$ can be computed from the moments

$$I_{ij} = M_{ij} - M_i M_j. \tag{4}$$

The three eigenvalues, $I_1$, $I_2$, and $I_3$, of the inertia tensor are directly related to the three principal axes of an ellipsoid fitted to the distribution of matter around the given point (fitting by an ellipsoid becomes increasingly accurate in the limit of small $R$ when the distribution can be approximated by a quadratic). Let us consider the ratios of the eigenvalues arranged in order of increasing magnitude, i.e., $I_1 \geq I_2 \geq I_3$:

$$\mu \equiv (I_2/I_1)^{1/2},\ \nu \equiv (I_3/I_1)^{1/2}. \tag{5}$$

The BS shape statistic consists of a triad of numbers ($S_1$, $S_2$, $S_3$) that can be constructed out of the parameters $\mu$ and $\nu$ as follows:

$$S_1 = \sin\left[\frac{\pi}{2}(1-\mu)^p\right],\ S_2 = \sin\left(\frac{\pi}{2}a\right),\ S_3 = \sin\left(\frac{\pi}{2}\nu\right), \tag{6}$$

where $p = \log 3/\log 1.5$; the function $a(\mu, \nu)$ is implicitly given by

$$\frac{\mu^2}{a^2} - \frac{\nu^2}{a^2(1 - \alpha a^{1/3} + \beta a^{2/3})} = 1, \tag{7}$$

where $\alpha = 1.9$ and $\beta = -(7/8)9^{1/3} + \alpha 3^{1/3}$. As a result, $0 \leq S_i \leq 1$, $i = 1, 2, 3$; i.e., the BS statistic can be thought of as a vector whose components are *always* positive and whose magnitude never exceeds unity. A perfectly spherical distribution has $I_1 = I_2 = I_3$, implying $\mu = \nu = 1$, $a = 0$, and $(S_1, S_2, S_3) = (0, 0, 1)$. Similarly, for a planar distribution $I_1 = I_2$, $I_3 = 0$, which implies $\mu = 1$, $\nu = 0$, and $a = 1$, so that $(S_1, S_2, S_3) = (0, 1, 0)$. A distribution that is filamentary has $I_2 = I_3 = 0$, so that $\mu = \nu = a = 0$ and $(S_1, S_2, S_3) = (1, 0, 0)$. Thus, the three components of the *shape vector* $\boldsymbol{S} = (S_1, S_2, S_3)$ represent filamentarity $S_1$, planarity $S_2$, and sphericity $S_3$. The magnitude and orientation of the shape vector describe some morphological properties of a distribution, for realistic distributions $S_i \neq 0$, $i = 1, 2, 3$. Since the three components of $\boldsymbol{S}$ depend only on two parameters $\mu$ and $\nu$, one can consider any two of them as being independent. In this work, we shall work mainly with $S_1$ (filamentarity/linearity) and $S_2$ (planarity); small values of both of these parameters imply a large value for sphericity $S_3$. We should point out that the moments in their present form can be used to determine shapes of continuous fields, such as brightness/temperature or density distributions, while those originally defined by BS could not have been used in such cases.

We now apply the BS shape statistic to overdense regions in a Wiener reconstruction of the *IRAS* 1.2 Jy redshift survey. The Weiner reconstruction method is useful in cosmology for constructing a real space density field from a galaxy distribution in redshift space that may be incomplete and sparsely sampled. The Weiner reconstruction technique uses linear perturbation theory to model and compensate for redshift space distortions caused by peculiar velocities of galaxies. The latter depend on the growth rate of the linear density contrast parameterized by $\beta = \Omega^{0.6}/b$, where $\Omega$ is the present value of the cosmic density parameter and $b$ is the linear bias parameter (for details of the Weiner reconstruction, see Rybicki & Press 1992 and Fisher et al. 1995a, 1995b). In this study, we investigate a set of three reconstructions of the *IRAS* density field corresponding to $\beta = 0.1$, 0.5, and 1.0. The real space density field is reconstructed on a $64^3$ grid with a side of 200 $h^{-1}$ Mpc (20,000 km $s^{-1}$).

Clusters in the *IRAS* survey are identified using percolation theory and a "friends-of-friends" algorithm on a grid that uses six nearest neighbors. A generic feature of any continuous density distribution (and therefore true also of the reconstructed *IRAS* density field) is that at very high thresholds, only a small

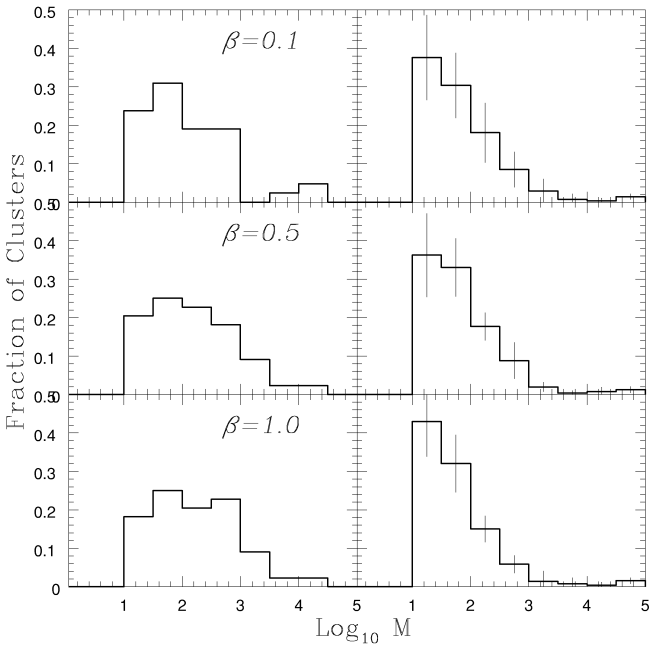


FIG. 1.—Multiplicity function of clusters in the *IRAS* 1.2 Jy redshift catalog (*left panels*). The multiplicity function for a Gaussian randomization of the *IRAS* catalog (*right panels*) is also shown.

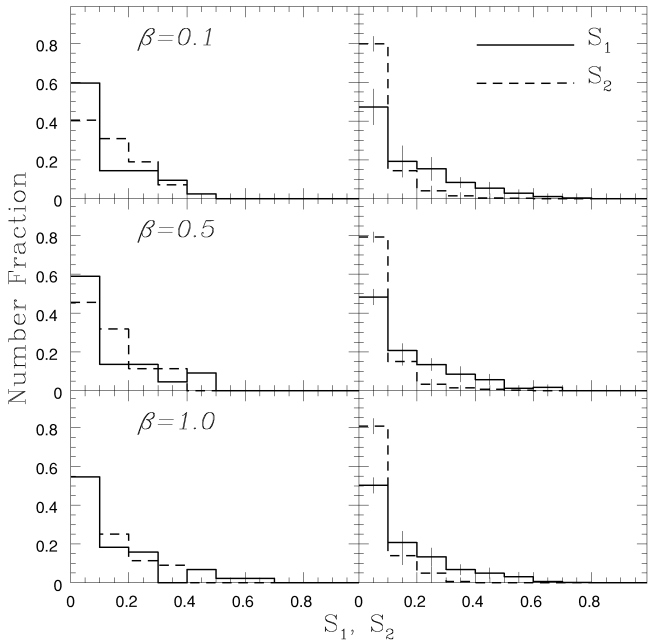


FIG. 2.—Shape spectrum of *IRAS* clusters (*left panels*) and of clusters from the randomized *IRAS* catalog (*right panels*).

volume is in the overdense phase, so that the resulting number of clusters is very small and so is the volume in the largest cluster. As the density threshold is lowered, the number of clusters increases, and the volume in the largest cluster grows rapidly because of the merging of nearby clusters. At a critical value of the density (the *percolation threshold*), the largest cluster percolates, spanning the entire region of interest in a homogeneous sample. Further lowering of the threshold increases mergers, resulting in a subsequent decrease in the number of clusters. Thus, the total number of clusters peaks at thresholds close to percolation, making the percolation transition an objective and useful density threshold at which to study properties of individual clusters (Sathyaprakash et al. 1996, 1998), and we shall use this threshold for studying cluster shapes in the *IRAS* survey. The density threshold at which the number of clusters peak for $\beta = 0.1$, 0.5, and 1.0 are $\rho_T =$ 1.59, 1.58, and 1.51, respectively.

The cluster multiplicity function for three reconstructions of the *IRAS* density field, $\beta = 0.1$, 0.5, and 1.0, is shown in Figure 1 (*left panels*). Gaussian randomized reconstructions of the *IRAS* catalog (*right panels*) are also shown, which serve as useful standards for our analysis. (Details of Gaussian randomization of the *IRAS* density field can be found in Yess et al. 1997.) In the *IRAS* catalog, there are between 40 and 50 clusters in each reconstruction. About half of them are small clusters, a third are of intermediate mass, and the rest are very massive. In a low-$\Omega$ universe, or if the bias is very large, the clusters tend to be not as massive as in a high-$\Omega$ universe, or if there is no biasing. The randomized *IRAS* catalog contains a larger fraction of small clusters as compared with the *IRAS* catalog. In our analysis, we have discarded clusters having a volume smaller than 8 grid cells since quantifying the shape of such clusters would be biased toward linearity/planarity because of a lack of resolution.

In Figure 2, we show the "shape spectrum," the number fraction of *IRAS* clusters having a given value of the BS shape parameters $S_1$ and $S_2$. From the shape spectrum, we see that

TABLE 1

CATALOG OF CLUSTERS/SUPERCLUSTERS FROM THE *IRAS* RECONSTRUCTION WITH $\beta = 0.5$

| *n* | *V* | *M* | ($S_1$, $S_2$, $S_3$) |
|---|---|---|---|
| 1 ..... | 10927 | 238 | (0.169, 0.005, 0.684) |
| 2 ..... | 1898 | 36 | (0.413, 0.082, 0.375) |
| 3 ..... | 1417 | 27 | (0.007, 0.388, 0.503) |
| 4 ..... | 905 | 17 | (0.493, 0.024, 0.394) |
| 5 ..... | 775 | 15 | (0.064, 0.221, 0.517) |
| 6 ..... | 494 | 10 | (0.419, 0.012, 0.465) |
| 7 ..... | 302 | 5.3 | (0.266, 0.199, 0.372) |
| 8 ..... | 302 | 5.1 | (0.204, 0.266, 0.367) |
| 9 ..... | 287 | 4.9 | (0.015, 0.104, 0.712) |
| 10 ..... | 232 | 4.4 | (0.113, 0.128, 0.541) |
| 11 ..... | 252 | 4.2 | (0.244, 0.271, 0.339) |
| 12 ..... | 239 | 4.2 | (0.200, 0.024, 0.597) |
| 13 ..... | 208 | 3.5 | (0.022, 0.376, 0.471) |
| 14 ..... | 197 | 3.3 | (0.067, 0.027, 0.728) |
| 15 ..... | 161 | 3.0 | (0.010, 0.051, 0.799) |
| 16 ..... | 165 | 2.8 | (0.064, 0.007, 0.795) |
| 17 ..... | 123 | 2.0 | (0.003, 0.107, 0.760) |
| 18 ..... | 117 | 1.9 | (0.066, 0.189, 0.539) |
| 19 ..... | 108 | 1.8 | (0.011, 0.293, 0.557) |
| 20 ..... | 97 | 1.6 | (0.047, 0.114, 0.635) |
| 21 ..... | 97 | 1.6 | (0.012, 0.017, 0.862) |
| 22 ..... | 93 | 1.5 | (0.280, 0.020, 0.540) |
| 23 ..... | 85 | 1.4 | (0.090, 0.239, 0.473) |
| 24 ..... | 73 | 1.2 | (0.122, 0.148, 0.515) |
| 25 ..... | 48 | 0.78 | (0.070, 0.188, 0.535) |
| 26 ..... | 38 | 0.78 | (0.006, 0.016, 0.886) |
| 27 ..... | 44 | 0.74 | (0.061, 0.019, 0.757) |
| 28 ..... | 37 | 0.59 | (0.208, 0.180, 0.422) |
| 29 ..... | 31 | 0.56 | (0.120, 0.016, 0.691) |
| 30 ..... | 32 | 0.53 | (0.399, 0.011, 0.482) |
| 31 ..... | 25 | 0.40 | (0.002, 0.180, 0.698) |
| 32 ..... | 24 | 0.39 | (0.047, 0.179, 0.573) |
| 33 ..... | 21 | 0.38 | (0.031, 0.047, 0.748) |
| 34 ..... | 23 | 0.37 | (0.035, 0.349, 0.465) |
| 35 ..... | 21 | 0.35 | (0.124, 0.003, 0.745) |
| 36 ..... | 17 | 0.27 | (0.052, 0.379, 0.422) |
| 37 ..... | 17 | 0.27 | (0.060, 0.024, 0.746) |
| 38 ..... | 16 | 0.27 | (0.320, 0.004, 0.569) |
| 39 ..... | 16 | 0.27 | (0.008, 0.040, 0.826) |
| 40 ..... | 15 | 0.25 | (0.482, 0.066, 0.351) |
| 41 ..... | 14 | 0.22 | (0.111, 0.190, 0.491) |
| 42 ..... | 11 | 0.18 | (0.000, 0.117, 0.799) |
| 43 ..... | 10 | 0.16 | (0.087, 0.117, 0.579) |
| 44 ..... | 9 | 0.14 | (0.083, 0.302, 0.437) |

NOTE.—The list contains many interesting structures, some of them quite massive and with significant amounts of planarity and/or filamentarity. The first column is the cluster number (*n*), the second is volume in grid units (*V*), and the third is mass/$10^2$ (*M*).

most *IRAS* clusters are predominantly isotropic/spherical; however, a small fraction can have fairly large amounts of planarity/filamentarity. Figure 2 does not provide a comprehensive picture since it weighs all clusters equally, regardless of whether they are large or small. The issue of the shape of the largest objects (superclusters) in the *IRAS* catalog is clearly one of central importance, and we explore it by showing the dependence of shape on mass in Figure 3. We find that for $\beta =$ 0.1, clusters in all mass ranges have almost equal amounts of planarity and filamentarity. However, for $\beta = 0.5$ and 1.0, the largest clusters (superclusters) tend to be predominantly filamentary, in agreement with the results of *N*-body simulations (Sathyaprakash et al. 1996, 1998). The statistical significance of these results is not yet clear because of the small number of such (large) objects in the *IRAS* survey volume, but a comparison with the randomized *IRAS* catalog (see the right panel of Fig. 3, in which results from 10 Gaussian randomizations

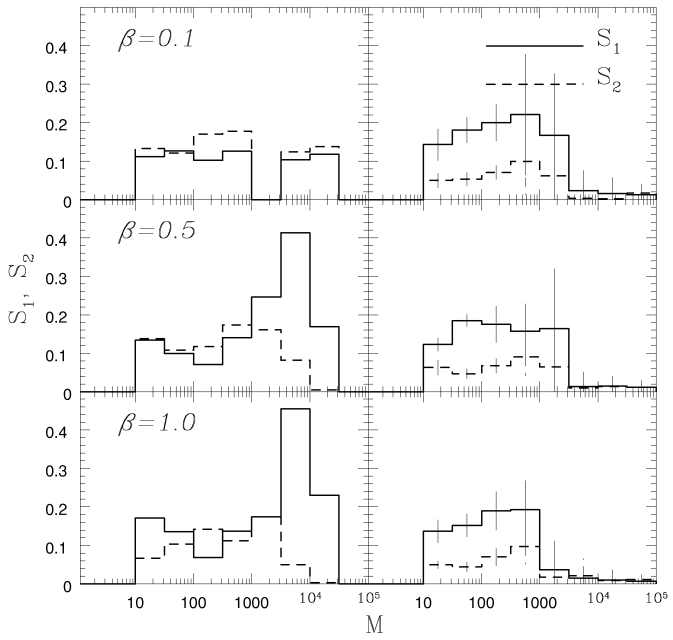


FIG. 3.—The dependence of shape on mass is shown for *IRAS* clusters (*left panels*) and for clusters chosen from the randomized *IRAS* catalog (*right panels*).

of the *IRAS* density field are shown) clearly indicates that very massive filamentary superclusters are extremely unlikely to appear "by chance." We also find that clusters in the randomized *IRAS* catalog are more prolate than oblate, in agreement with the earlier analysis of the shapes of density peaks in a Gaussian random field (Bardeen et al. 1986; Dubinsky 1992; Peacock & Heavens 1985).

Table 1 is our catalog of clusters in the *IRAS* density fields reconstructed with $\beta = 0.5$. (We do not include very small clusters having a volume less than 8 grid cells.) We find several large clusters with significant amounts of filamentarity/planarity. It should be pointed out that the largest "percolating" supercluster is likely to be "treelike," with several branches emanating from a "central trunk." This will give it an isotropic appearance on very large scales. Since the BS statistic is moment-based, it is likely to interpret such an isotropic structure as being spherical! This shortcoming of moment-based shape statistics can be avoided if one works with shape diagnostics based on Minkowski functionals, as demonstrated in Sahni, Sathyaprakash, & Shandarin (1998) and Sathyaprakash et al. (1998). (In addition, clusters occurring at the edge of the box may show enhanced planarity because of boundary effects.)

To conclude, we have addressed the issue of the morphology of clusters and superclusters in the *IRAS* 1.2 Jy redshift catalog. We find that individual clusters defined at the percolation threshold can have significant amounts of both filamentarity and planarity, the largest clusters appearing to be strongly filamentary. Although these results are broadly in agreement with recent studies of *N*-body simulations, their statistical implications are still unclear, mainly because of the sparseness of the *IRAS* catalog. However, the stage is now set to analyze larger and deeper three-dimensional redshift surveys complementing the *IRAS* survey, such as the 2dF and the SDSS. A comprehensive study of cluster and supercluster shapes in these surveys is bound to shed more light on the abundance of pancakes, filaments, and ribbons and on the geometry of large-scale structure, whether bubble-like, network-like, or some other!

B. S. S. acknowledges the support of NSF grant AST-9417371 and thanks Kip Thonre for the hospitality at the California Institute of Technology, where this work began. S. Shandarin acknowledges the support of NASA grant NAG 5-4039 and an EPSCoR 1998 grant.

REFERENCES

Babul, A., & Starkman, G. D. 1992, ApJ, 401, 28 (BS)
Bardeen, J. M., Bond, J. R., Kaiser, N., & Szalay, A. S. 1986, ApJ, 304, 15
Bond, J. R., Kofman, L., & Pogosyan, D. 1996, Nature, 380, 603
de Lapparent, V., Geller, M. J., & Huchra, J. P. 1991, ApJ, 369, 273
Dubinsky, J. 1992, ApJ, 401, 441
Fisher, K. B., Huchra, J. P., Strauss, M. A., Davis, M., Yahil, A., & Schlegel, D. 1995a, ApJS, 100, 69
Fisher, K. B., Lahav, O., Hoffman, Y., Lynden-Bell, D., & Zaroubi, S. 1995b, MNRAS, 272, 885
Klypin, A. A., & Shandarin, S. F. 1993, ApJ, 413, 48
Peacock, J. A., & Heavens, A. F. 1985, MNRAS, 217, 805
Rybicki, G. B., & Press, W. H. 1992, ApJ, 398, 169
Sahni, V., & Coles, P. 1995, Phys. Rep., 262, 1
Sahni, V., Sathyaprakash, B. S., & Shandarin, S. F. 1998, ApJ, 495, L5
Sathyaprakash, B. S., Sahni, V., & Shandarin, S. F. 1996, ApJ, 462, L5
———. 1998, ApJ, in press
Shandarin, S. F., Melott, A. L., McDavitt, A., Pauls, J. L., & Tinker, J. 1995, Phys. Rev. Lett., 75, 7
Shandarin, S. F., & Zeldovich, Ya. B. 1989, Rev. Mod. Phys., 61, 185
Yess, C., & Shandarin, S. F. 1996, ApJ, 465, 2
Yess, C., Shandarin, S. F., & Fisher, K. B. 1997, ApJ, 474, 553
Zeldovich, Ya. B., Einasto, J., & Shandarin, S. F. 1982, Nature, 300, 407